Research on Image Detection and Recognition for Defects on the Surface of the Steel Plate Based on Magnetic Flux Leakage Signals

Wang Ze-song

Institute of Petroleum and Chemical, Shenyang University of Technology，Shenyang 110870，China

E-mail: 22729883@163.com

Abstract：In order to improve CCD recognition accuracy for defection on the steel plate surface caused by illumination uniformity of light source, light color, impact of site environmental and the low signal-to-noise ratio images on the surface of the steel plate collected by the system, this paper proposes a new image process and BP neural network detection recognization method based on magnetic flux leakage data in order to realize accurate and effective identification on the surface of steel plate. In this paper, non-destructive magnetic flux leakage detection technology is used to replace the CCD detection method to collect data. And then we use the image conversion technology to convert the data into images. After that, the image processing technology is used to detect the defects and extract the features. Finally, the BP neural network defect identification model is constructed to identify the defects. The simulation results show that the trained model has a strong ability to recognize length, width and depth of the defects. The new method can effectively detect and identify low-contrast and small defects in the weak signal, which can furtherly improve the detection resolution and sensitivity.

Key words：Defect recognition；Wavelet transform；Multi-scale edge detection；Feature extraction；BP neural network

1 Introduction

Steel has become indispensable raw materials of machinery manufacturing, automobile manufacturing, chemical industry, ship building, aerospace and other industries, which occupies the important position in the national economy[1-3]. However, there are often different types of quality defects on the surface of the steel plate, due to rolling equipment, continuous casting billets, processing and many other reasons. As a result of the existence of these defects, productions produced by the steel plate will exist safe hidden trouble, which not only affects the use of the products, but also even can cause huge losses to the national economy and the harm to safety of personal property.

In recent years, the technology of steel plate surface defect detection as the core with machine vision technology has become the focus and trend of the current research[4-6], with the development of computer technology and automation technology, as well as the maturity of artificial intelligence and neural network theory. Since the 90s, the CCD and digital image processing system developed by the Italian company SIPAR and North American ISYS control equipment company is suitable for testing defect on the surface of a variety of material. However, the optical path configuration, resolution and sensitivity still need to be improved[7][8]. More worse, the signal-to-noise ratio of the detection system is too low and the system lacks the corresponding method for recognizing the small and low-contrast defect. Besides, it lacks high-speed, massive digital signal processing platform, image processing and pattern recognition algorithm. Although the CCD detection and digital image processing method developed by Hoogovens (EES) of Holland is suitable for detecting hot rolling environments, the resolution is low and does not have non-identification part. Compared with foreign countries, domestic researches on steel plate surface defect detection start relatively late. In the early 90s, Luo Shying used laser scanning method to detect and identify hole defects on the cold-rolled steel plate, and designed the corresponding signal processing circuit. After that, he studied detection technology of line CCD and area CCD[9]. They developed a multi-plane array CCD imaging technology in 1995 and used it to test surface hole, edge crack and heavy skin of cold

rolled steel sheet. At the same time, Harbin robotics technology Institute made a study of static detection and recognition of main defects on steel plate surface.

A key factor in determining the accuracy of the recognition is the images, which are usually captured by a CCD camera. But due to the light source illumination uniformity, colour and light environment on site and the signal-to-noise ratio of the steel plate surface image acquired by the system is very low. While the defect area is small and the shape is not regular, the difference between all kinds of the characteristics is not obvious. Therefore, defect recognition rate of steel surface is difficult to improve.

In this paper, non-destructive magnetic flux leakage detection technology is used to replace the CCD detection method to collect data, and then we use the image conversion technology to convert the data into images. After that, the image processing technology is used to detect the defects and extract the features. Finally, the BP neural network defect identification model is constructed to identify the defects. The extracted feature quantity is used as an input quantity, and the established model is trained by using the known corresponding sample data. And then we validate the model with unknown sample data. The simulation shows that the trained model can identify length, width and depth of the defects effectively. The advantage of our method is that the detection resolution and sensitivity are furtherly improved, and the low-contrast and small defects in the weak signal can be detected.

2 Imaging processing of Magnetic flux leakage data

A one-dimensional curve is the most common way of graphical display for the magnetic flux leakage data, and can indicate the change trend of the magnetic flux leakage signal through the ups and downs of the curve, which is the most important basis for follow-up analysis of magnetic flux leakage defects.

2.1 Base Correction and Interpolation of Magnetic Flux Leakage Data

The magnetic flux leakage data collected in the field is detected by multiple sensors. Due to the influence of each sensor itself as well as various other factors, for instance, each magnetic flux leakage sensor has different characteristics, as well as analog channel amplification amplifier circuit is inconsistent, the probe installation error and other factors. Hence, the magnetic flux leakage data for the same defect will inevitably exist some deviation and there will be inconsistencies on the measurement standards. The collected data is shown in figure 1. Therefore, it is necessary to correct deviation between each channel, which lays a good foundation for the subsequent data processing.
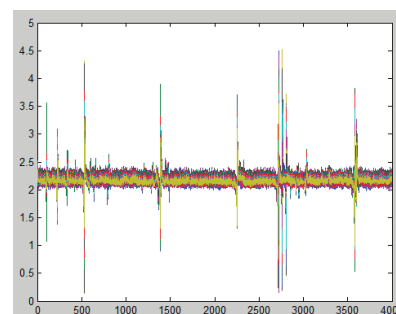

Fig. 1 The original leakage magnetic curve

First of all, we perform base value correction for collected leakage flux data, the steps of the correction method are as follows：

Step one. Take the median value of the magnetic flux leakage data from each sensor.

Step two. Take the mean value obtained in step one is as a reference value.

Step three. Take the reference value as the origin. The offset calibration is performed according to the median value of the data collected by each sensor：The data value collected by each sensor is subtracted from the median value of the data collected by the corresponding sensor, and then the reference value is

added to complete the calibration process.

After that, the cubic spline method is used to interpolate on data to obtain the processed data. The magnetic flux leakage curves after processed are shown in Fig.2.
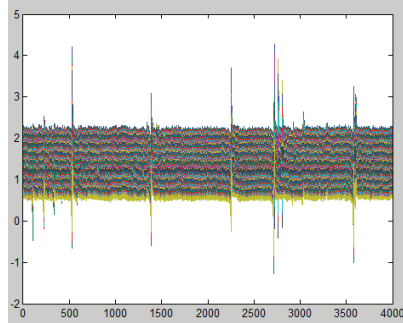

Fig. 2 The magnetic flux leakage curves after processed

2.2 Image conversion for the magnetic flux leakage data

The defect gray-scale image is another expression of the magnetic flux leakage data curve. The different data values are represented by the corresponding gray levels. Take the gray level, perimeter, area and other information of the image as a characterization of the defect, which corresponds to the amplitude, slope, and gradient of the data curve. Obviously, the larger the size and the darker the area is, the more serious the defect is, which corresponds to the maximum amplitude region of the magnetic flux leakage data curve.

The data we collected in our experiments were 16-bit double-precision, what's more the numerical range is in the range of 0-255. We firstly convert the data to the range of 0-255. This is because the data sampling accuracy is not enough high, and the gray scale between the defects and the normal wall is not obvious, and the data span is not large. Therefore it is necessary to adjust data.

Steps of adjusting the data to a scale of 0-255 are as follows：

Step one. Calculate the excess ratio S between the current magnetic flux leakage data and the median value of the data collected by the corresponding sensor：

$$S = (X - M) / M \tag{1}$$

Among it, X is the current magnetic flux leakage data collected by the sensor；M is the median value of the data collected by the corresponding sensor.

Step two. Subject the data calculated in the previous step to the constraint range：

$$S = \begin{cases} -1 & S \le -1 \\ 1 & S \ge 1 \end{cases} \tag{2}$$

Step three. Convert the data collected by each sensor to the corresponding gray value：

$$128 - 128 * S \tag{3}$$

Step four. Convert the data obtained in step three into integer data range of 0-255.

The processing of the out-of-range constraint is performed through the step two, which makes sure that the gray scale values obtained by the conversion in step three are between 0 and 255. However, the gray values obtained by the above steps are not all integers. So we should also do integer conversion processing to the data. The preliminary gray scale image generated by the conversion is shown in Fig. 3.

Fig. 3 Preliminary gray scale image

3 Edge detection and feature extraction of defects

3.1 The edge of the image

Although the edge points of the image are generated for different reasons, they are all the discontinuity or sharply change points of the gray image. Apparently it is some fuzzy to be said so that. Therefore, it is necessary to define a relatively precise mathematical model of the edge.

Suppose that $f(u,v)$ represents a continuous image, and the gradient vector is defined as follows:

$$\nabla f = (\frac{\partial f}{\partial u}, \frac{\partial f}{\partial v}) \qquad (4)$$

The gradient vector shows that $f(u,v)$ is maximum change direction at the point of (u,v).

Suppose that (u_1,v_1) is the point on the image, if $|\nabla f| = \sqrt{\left|\frac{\partial f}{\partial u}\right|^2 + \left|\frac{\partial f}{\partial v}\right|^2}$ is gradient vector of f, $(u,v) = (u_1,v_1) + \lambda \nabla f(u_1,v_1)$ changes along the direction of maximum variation at the point of (u_1,v_1), when $|\lambda|$ is sufficiently small to take the local maximum at that point, then we call (u_1,v_1) is an edge point of $f(u,v)$.

3.2 Edge detection of defects

In spite that traditional or modern image edge detection methods are accurate for edge location of the traditional image, but they can't accurately detect the edge of defects for the magnetic flux leakage image. On the contrary, wavelet multi-scale edge detection method can accurately locate the location of the edge of defects.

Suppose that two-dimensional smoothing function $\theta(u,v)$ satisfies the following conditions:

$$\theta(u,v) \geq 0, \qquad \iint_{R^2} \theta(u,v)dudv = 1, \qquad \lim_{u,v \to \pm\infty} \theta(u,v) = 0$$

$$\theta_{2^j}(u,v) = \frac{1}{2^{2j}}\theta(\frac{u}{2^j}, \frac{v}{2^j}) \qquad (5)$$

then for any $f(u,v) \in L^2(R^2)$, $(f * \theta_{2^j})(u,v)$ represents the image that $f(u,v)$ is smoothed by $\theta_{2^j}(u,v)$, among it 2^j is the smooth scale.

We define two two-dimensional wavelets by using $\theta(u,v)$:

$$\psi^1(u,v) = \frac{\partial \theta(u,v)}{\partial u}, \ \psi^2(u,v) = \frac{\partial \theta(u,v)}{\partial v}$$

$$\psi^1_{2^j}(u,v) = \frac{1}{2^{2j}}\psi^1(\frac{u}{2^j}, \frac{v}{2^j}), \ \psi^2_{2^j}(u,v) = \frac{1}{2^{2j}}\psi^2(\frac{u}{2^j}, \frac{v}{2^j}),$$

then two-dimensional wavelet transform of the image $f(u,v)$ on the scale of 2^j is as follows:

$$W^1 f(2^j,u,v) = \iint_{R^2} f(x,y)\frac{1}{2^j}\psi^1(\frac{x-u}{2^j}, \frac{y-v}{2^j})dxdy = 2^j(f * \overline{\psi}^1_{2^j})(u,v) \qquad (6)$$

$$W^2 f(2^j,u,v) = \iint_{R^2} f(x,y)\frac{1}{2^j}\psi^2(\frac{x-u}{2^j}, \frac{y-v}{2^j})dxdy = 2^j(f * \overline{\psi}^2_{2^j})(u,v) \qquad (7)$$

Among them, $\overline{\psi}^k_{2^j}(u,v) = \psi^k_{2^j}(-u,-v), k=1,2$.

Because the modulo value $\nabla(f * \overline{\theta}_{2^j})(u,v)$ of the gradient vector $(f * \overline{\theta}_{2^j})(u,v)$ is proportional to the following wavelet transform:

$$Mf(2^j,u,v) = \sqrt{\left|W^1 f(2^j,u,v)\right|^2 + \left|W^2 f(2^j,u,v)\right|^2} \qquad (8)$$

and the angle between the gradient direction and the horizontal direction u is as follows:

$$Af(2^j,u,v) = \arctan\left(\frac{W^2 f(2^j,u,v)}{W^1 f(2^j,u,v)}\right) \qquad (9)$$

so calculating modulus maxima value of a polished function $(f * \overline{\theta}_{2^j})(u,v)$ along the gradient direction is equivalent to calculate modulus maxima value of two-dimensional binary wavelet transform. It is easy to prove that the edge points of the image can be determined by detecting the modulus maxima of the 2D wavelet transform.

Suppose that D has $N \times N$ pixels, steps of wavelet multi-scale modulus maxima edge detection are as follows:

On the scale of 2^j, calculate two-dimensional wavelet transform of image D according to (6) and (7).

Calculate modulus and phase angle of each point according to (8) and (9).

The modulus maxima of the wavelet coefficients in each layer are determined by using 8-neighborhood.

If modulus of a point in each wavelet transform is the local maximum value, and its amplitude increases with the scale, then the point is the true edge point; otherwise, it is not an edge point. Mark the edge point as 1 and the non-edge point as 0. Finally extract a binary image only containing edge features as shown in Fig.4.
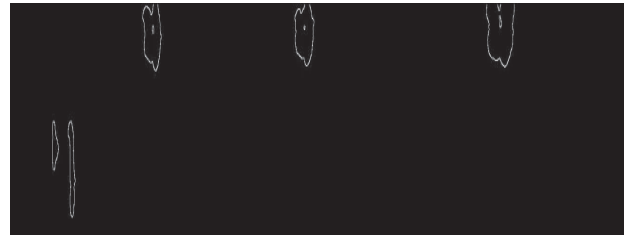

Fig.4 A binary image with only edge features

It can be can clearly seen from fig.4 that there are five defects. We can clearly see the shape of defects.

3.3 Feature extraction of defects

Extract the information of the defect geometric feature such as the long axis, short axis, circumference,

area and eccentricity of the defect from the defective edge binary image. The information of the defect geometric feature is shown in Table 1.

Table 1 The information of the defect geometric feature

Seril number	Long axis /mm	Short axis /mm	perimeter /mm	area /mm^2	Eccentricity
1	49.55	58.21	166	2081	0.8512
2	69.00	60.71	231	3387	1.1366
3	16.00	46.00	97	456	0.3478
4	14.18	89.09	183	876	0.1592
5	44.58	63.10	180	2111	0.7065

4 Predictive model of neural network

4.1 Establishment of BP neural network model

In this paper, there are five kinds of input, so the number of neurons in the input layer is five. We use two hidden layers for training. The number of the first and second hidden layer is five and ten respectively. There are three kinds of output, so the number of neurons in the output layer is three[10-12].

4.2 Training of BP Neural Network Model

Take tansig as the transfer function of the hidden layer and purelin as transfer function of the output layer. The network structure of the defect identification model is 5×5×10×3. The learning rate determines the change rate of weights produced in each cycle of training. Large learning rate may lead to instability of the system, but the small learning rate will lead to the longer training time and can't guarantee that the error value of the network jump out of the trough of the error surface and eventually tends to be the minimum error value[13-15]. The learning rate is chosen from 0.01 to 0.8. In this model, the learning rate is 0.05, the mean square error is 0.005 and the maximum iteration number is 500.

The convergence curve of the network in the training process is shown in Fig.5. It can be seen that network achieves convergence after training 273 steps from the Fig.5.
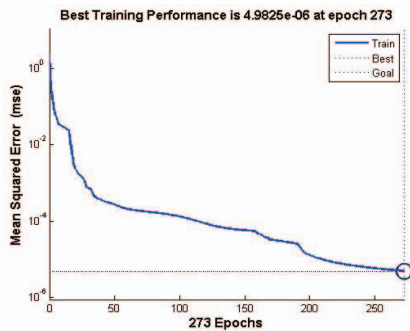

Fig.5 The training convergence curve

Table 2 Training results of defect length

Seril number	Training length /mm	Actual length /mm	Absolute error /mm	Relative error rate
1	9.5874	10	0.4126	4.13%
2	19.2741	20	0.7259	3.63%
3	4.8842	5	0.1158	2.32%
4	9.5673	10	0.4327	4.33%
5	14.589	15	0.411	2.74%

Table 2 is the training results of the defect length. The average relative error rate is 3.43%. It can be concluded that the predicted length value and the actual length value almost exactly match. We can say this neural network satisfies the requirement of length prediction according to the calculated average relative error rate.

Table 3 Training results of defect width

Seril number	Training width/mm	Actual width /mm	Absolute error /mm	Relative error rate
1	4.7235	5	0.2765	5.53%
2	20.3186	20	0.3186	1.59%
3	9.4215	10	0.5785	5.79%
4	9.5407	10	0.4593	4.59%
5	9.6369	10	0.3631	3.63%

Table 3 is the training results of the defect width. The average relative error rate is 4.23%. It can be concluded that the predicted width value and the actual width value almost exactly match. This neural network also satisfies the requirement of width prediction.

Table 4 Training results of defect depth

Seril number	Training depth /mm	Actual depth /mm	Absolute error /mm	Relative error rate
1	1.1213	1	0.1213	12.13%
2	3.7621	4	0.2379	5.95%
3	3.1862	3	0.1862	6.21%
4	8.8126	9	0.1874	2.08%
5	3.8532	4	0.1468	3.67%

Table 4 is the training results of the defect depth. The average relative error rate is 6.01%. It can be concluded that the predicted depth value and the actual depth value almost exactly match. Therefore, this neural network satisfies the requirement of depth prediction.

4.3 Prediction of BP Neural Network Model

Using the trained BP neural network defect identification model above to predict the information of the unknown defect in Table 1, the identification results of length, width and depth are shown in Table 5.

Table 5 Prediction results of the defect

Seril number	Identification length /mm	Identification width /mm	Identification width /mm
1	14.5984	15.3362	3.5983
2	25.3192	4.7963	1.7534
3	10.2506	10.2264	3.6978
4	14.6981	29.7948	1.1315
5	20.3337	9.6744	5.7835

5 Conclusion

In this paper, analogying CCD detection method

and digital image processing technology, we first convert data into a grayscale image after base value correction and data interpolation. Then, the edge of the defect in the gray image is detected by the edge detection method based on the wavelet multi-scale modulus maxima value, and the defective edge binary image is used to detect the geometric features of the defect gray image (long axis, short axis, circumference, area, and eccentricity). Finally, a defect network identification model is established by using BP neural network, and trained by the sample data. The trained defect identification model is validated by known data from the absolute error and relative error rate respectively. The identification results show that the defect identification model can effectively identify the length, width and depth of the defects.

Acknowledgments

References

[1] Petcher P A, Dixon S. Weld defect detection using PPM EMAT generated shear horizontal ultrasound[J]. Ndt&E International, 2015, 8:58-65.

[2] Liu B, Cao Y, Zhang H, et al. Weak magnetic flux leakage: A possible method for studying pipeline defects located either inside or outside the structures[J]. Ndt & E International, 2015, 74:81-86.

[3] Gao B, Woo W L, He Y, et al. Unsupervised Sparse Pattern Diagnostic of Defects With Inductive Thermography Imaging System[J]. IEEE Transactions on Industrial Informatics, 2015, 12(1):371-383.

[4] Ahanian I, Sadeghi S H H, Moini R. An array waveguide probe for detection, location and sizing of surface cracks in metals[J]. Ndt & E International, 2015, 70:38-40.

[5] R Jin，J Yin，W Zhou，J Yang. Improved Multiscale Edge Detection Method for Polarimetric SAR Images[J]. IEEE Geoscience and Remote Sensing Letters, 2016, 13(8):1104-1108.

[6] Florez-Ospina J F, Benitez-Restrepo H D. Toward images of composites and honeycomb structures[J]. Infrared Physics & Technology, 2015, 71:99-112.

[7] Hu Y, Chen J, Pan D, et al. Edge-Guided Image Object Detection in Multiscale Segmentation for High-Resolution Remotely Sensed Imagery[J]. IEEE Transactions on Geoscience & Remote Sensing, 2016, 54(8):4702-4711.

[8] Fatan M, Daliri M R, Shahri A M. Underwater Cable Detection in the Images using Edge Classification based on Texture Information[J]. Measurement, 2016, 91:309-317.

[9]Tang Q, Dai J, Liu J, et al. Quantitative detection of defects based on Markov–PCA–BP algorithm using pulsed infrared thermography technology[J]. Infrared Physics &Technology,2016, 77:144-148.

[10]He Y L, Wang X, Zhu Q X. Modeling of acetic acid content in purified terephthalic acid solvent column using principal component analysis based improved extreme learning machine[J]. Control Theory & Application, 2015, 32(1): 80-85.

[11] Huang G B. Extreme learning machine for regression and multiclass classification[J]. IEEE Trans on Systems, 2012, 42(2): 513-516.

[12]Ding G, Zhong S S. Time series prediction based on process neural networks and its applications[J]. Control and Decision, 2006, 21(9): 1037-1041.

[13] Long B, Jiang XW, Song Z J, et al. Study for multiple fault diagnosis technology for spacecrafts based on multi-signal model[J]. J of Astronautics, 2004, 25(5): 591-594.

[14]Ding G, Zhong S S. Time series prediction based on process neural networks and its applications[J]. Control and Decision, 2006, 21(9): 1037-1041.

[15]Wang C,Wang J H. Improved hybrid incremental extreme learning machine algorithm[J]. Control and Decision, 2015, 30(11): 1982-1985.